Enhanced Cross-Phase Modulation Based on a Double Electromagnetically Induced Transparency in a Four-Level Tripod Atomic System

Shujing Li, Xudong Yang, Xuemin Cao, Chunhong Zhang, Changde Xie, and Hai Wang*

The State Key Laboratory of Quantum Optics and Quantum Optics Devices, Institute of Opto-Electronics, Shanxi University, Taiyuan 030006, People's Republic of China

(Received 3 February 2008; published 13 August 2008)

We report experimental observations on the simultaneous electromagnetically induced transparency (EIT) effects for probe and trigger fields (double EIT) as well as the enhanced cross-phase modulation (XPM) between the two fields in a four-level tripod EIT system of the $D1$ line of ^{87}Rb atoms. The XPM coefficients (larger than 2×10^{-5} cm^2/W) and the accompanying transmissions (higher than 60%) are measured at a slight detuning of the probe field from the exact EIT-resonance condition. The system and enhanced cross-Kerr nonlinearities presented here can be applied to quantum information processes.

DOI: 10.1103/PhysRevLett.101.073602 PACS numbers: 42.50.Gy, 32.80.−t, 42.65.−k

Cross-Kerr nonlinearity, or the so-called cross-phase modulation (XPM), has received more attention since it can find applications in demonstrating quantum phase gates (QPG) [1–3], generating quantum entanglement of single photons [4], constructing a near deterministic controlled-NOT gate [5], and performing a nondestructive Bell-state detection [6]. However, the absence of sufficient XPM in conventional media becomes an obstacle to its applications in quantum information processing (QIP). Electromagnetically induced transparency (EIT) technology is a promising avenue for solving the problem [2–4]. The large cross-Kerr nonlinearity in a four-level N-type EIT system has been theoretically proposed [7] and experimentally demonstrated in cold atoms [8]. However, in the N-type EIT system, the large cross-Kerr nonlinearity between probe and trigger (signal) pulses may not occur due to their group velocity mismatching [9–11]. Recently, several schemes have been proposed to obtain a large XPM based on the simultaneous EIT for two weak fields in various multilevel systems [2,3,10,11]; that is because in this case the group velocity matching will be possible, thus the long interacting time for producing a large XPM can be obtained. Until now, to the best of our knowledge, the experimental demonstration of a large XPM effect between two weak fields based on double EIT has not been presented. The experimental search for the effect is highly anticipated. Under this motivation we carried out this experimental study.

In this Letter, we report the first experimental observations on double EIT and the enhanced cross-phase modulation between the two fields in a four-level tripod EIT system of the $D1$ line of ^{87}Rb atoms. The relevant atomic levels are shown in Fig. 1 of Ref. [12]. The probe field E_P of frequency ω_P is left circularly polarized (σ^-), with a Rabi frequency $\Omega_p = \mu E_p/\hbar$, coupling between the transitions from levels $|a_{i+1}\rangle$ to $|e_i\rangle$ ($i = 1, 2$). The coupling field E_C of frequency ω_C is also σ^- polarized, with a Rabi frequency $\Omega_C = \mu E_c/\hbar$, to drive the levels $|b_{i+2}\rangle$ to $|e_i\rangle$ transitions ($i = 1, 2, 3$). The trigger field E_T of frequency ω_T is right circularly polarized (σ^+), with a Rabi frequency $\Omega_T = \mu E_T/\hbar$, coupling to the levels $|b_i\rangle$ to $|e_i\rangle$ transitions ($i = 1, 2, 3$). μ is the dipole moment for ^{87}Rb $D1$ transitions. In this case, the system is coherently prepared into two four-level tripod-type systems [12]. One is formed by the levels $|a_2\rangle - |b_3\rangle - |b_1\rangle - |e_1\rangle$ and the other by the levels $|a_3\rangle - |b_4\rangle - |b_2\rangle - |e_2\rangle$. The σ^- probe transition and σ^+ trigger transition share a common excited state $|e_1\rangle$ ($|e_2\rangle$), which induces a coupling between the probe and trigger fields in such a coherently prepared tripod system, so that the cross-Kerr phase modulation between the two fields will be enhanced. The total probe (trigger) susceptibility χ_p (χ_T) should include the contributions of both systems; that is, $\chi_P = \chi_{P1} + \chi_{P2}$ ($\chi_T = \chi_{T1} + \chi_{T2}$). In the presented measurement of the XPM between the probe and trigger beams, the condition of $|\Omega_{P,T}|^2 \ll |\Omega_C|^2$ is satisfied. Solving the density-matrix equations of Eq. (3) in Ref. [12] for these conditions, under the steady-state condition [2,3], the susceptibilities χ_{pi} ($i = 1, 2$) and χ_{Ti} ($i = 1, 2$) are obtained:

$$\chi_{Pi} = \frac{N|\mu_{ai+1,ei}|^2}{\hbar\varepsilon_0}\left\{\frac{\rho_{ai+1,ai+1} - \rho_{ei,ei}}{-\tilde{\Delta}_P + |\Omega_{Ti}|^2/4\tilde{\Delta}_{PT} + |\Omega_{Ci}|^2/4\tilde{\Delta}_{PC}} - \frac{|\Omega_{Ti}|^2(\rho_{bi,bi} - \rho_{ei,ei})/4}{-\tilde{\Delta}_{PT}(-\tilde{\Delta}_T^* + |\Omega_{ci}|^2/4\tilde{\Delta}_{TC}^*)(-\tilde{\Delta}_P + |\Omega_{Ci}|^2/4\tilde{\Delta}_{PC})}\right\}, \quad (1a)$$

$$\chi_{Ti} = \frac{N|\mu_{bi,ei}|^2}{\hbar\varepsilon_0}\left\{\frac{\rho_{bi,bi} - \rho_{ei,ei}}{-\tilde{\Delta}_T - |\Omega_{Pi}|^2/4\tilde{\Delta}_{PT}^* + |\Omega_{Ci}|^2/4\tilde{\Delta}_{TC}} - \frac{|\Omega_{Pi}|^2(\rho_{ai+1,ai+1} - \rho_{ei,ei})/4}{\tilde{\Delta}_{PT}^*(-\tilde{\Delta}_P^* + |\Omega_{ci}|^2/4\tilde{\Delta}_{PC}^*)(-\tilde{\Delta}_T + |\Omega_{Ci}|^2/4\tilde{\Delta}_{TC})}\right\}, \quad (1b)$$

where $\tilde{\Delta}_P = \Delta_P + i\gamma_0$, $\tilde{\Delta}_T = \Delta_T + i\gamma_0$, $\tilde{\Delta}_{PT} = \Delta_P - \Delta_T + i\gamma_1$, $\tilde{\Delta}_{PC} = \Delta_P - \Delta_C + i\gamma_2$, $\tilde{\Delta}_{TC} = \Delta_T - \Delta_c + i\gamma_3$, and Δ_P, Δ_C and Δ_T are the probe, coupling, and trigger frequency detunings [12], respectively. γ_j ($j = 0, 1, 2, 3$) describes decay of populations and coherences. $\rho_{ai,ai}$, $\rho_{bi,bi}$, and $\rho_{ei,ei}$ are the populations of states $|a_i\rangle$, $|b_i\rangle$, and $|e_i\rangle$, respectively.

$\Omega_{Pi} = \Omega_P C_{ei,ai+1}$, $\Omega_{Ci} = \Omega_C C_{ei,bi+2}$, and $\Omega_{Ti} = \Omega_T C_{ei,bi}$ are the probe, coupling, and trigger Rabi frequencies for the transitions from Zeeman levels $|a_{i+1}\rangle$ to $|e_i\rangle$, $|b_{i+2}\rangle$ to $|e_i\rangle$, and $|b_i\rangle$ to $|e_i\rangle$, respectively. $C_{ei,bj(ak)}$ is a coefficient related to the dipole moment $\mu_{ei,bj(ak)}$ for the transition from level $|b_j\rangle$ ($|a_k\rangle$) to $|e_i\rangle$ with a expression $\mu_{ei,bj(ak)} = C_{ei,bj(ak)}\mu$. For comparing the cross-Kerr nonlinearity produced from the four-level tripod systems with and without EIT, we respectively calculated the XPM coefficients in the two different systems from Eqs. (1). For the EIT scheme, the calculated XPM coefficients are $n^{(2)}_{P,E} \approx 4.2 \times 10^{-6}$ cm^2/W and $n^{(2)}_{T,E} = 7.3 \times 10^{-6}$ cm^2/W for $\Omega_C = 70$ MHz and $\Omega_P = \Omega_T = 6$ MHz, respectively, and with a slight probe detuning $\Delta_P \approx -0.5$ MHz from EIT-resonance ($\Delta_C = \Delta_T = \Delta_P = 0$). The accompanying probe and trigger absorptions are 42% and 57%, respectively. However, in the conventional scheme, if the probe (trigger) absorption equals ~42% (~57%), the system has to operate at the large detunings of $\Delta_P \approx -200$ MHz and $\Delta_T \approx 200$ MHz to avoid the very strong resonance absorption. In this case, the calculated XPM coefficients are $n^{(2)}_{P,C} = 3.78 \times 10^{-9}$ cm^2/W and $n^{(2)}_{T,C} = 0.94 \times 10^{-9}$ cm^2/W, respectively. The calculation shows that the EIT enhancement factors of $n^{(2)}_{P,E}/n^{(2)}_{P,C} \approx 1000$ and $n^{(2)}_{T,E}/n^{(2)}_{T,C} \approx 5000$ are achieved in the presented scheme.

Figure 1 depicts the experimental setup. LD1 (for probe beam) and LD2 (for coupling and trigger beams) are the frequency-stabilized diode lasers (linewidths ~ 1 MHz) with grating feedback. The LD2 laser beam is split into two parts by a beam splitter (BS1). One of them serves as the trigger beam, and the other one serves as the coupling beam. The trigger beam passes through an acousto-optical modulator system for scanning its frequency around ω_{be} (see Ref. [12] for the details). The EIT dispersion curves of the probe and trigger beams are measured with a common Mach-Zehnder interferometer. The Mach-Zehnder interferometer consists of two beam displacing polarizers, BD1 and BD2, which play the role of the two beam splitters used in Fig. 2 of Ref. [13]. The linearly polarized input probe beam (with a chosen polarization angle) is separated into two orthogonally polarized beams, s- and p-polarized beams, by BD1. They are used for the probe and the probe reference beams, and they copropagate along line L_2 and line L_1, respectively. Similarly, the linearly polarized input trigger beam is also separated into orthogonal s- and p-polarized output beams by BD1. The p-polarized trigger beam propagates along line L_2 and overlaps with the s-polarized probe beam. The s-polarized trigger reference beam propagates along line L_3, which is parallel with line L_2. The s-polarized coupling beam propagates through a Rb cell with a small angle (~1°) relative to line L_2 and overlaps with the probe and trigger beams inside the Rb cell. The s-polarized probe and coupling beams become σ^- polarized, while the p-polarized trigger beam becomes σ^+ polarized after they respectively pass through a $\lambda/4$ wave plate. The length of the atomic cell without buffer gas is $l =$ 50 mm with magnetic shielding, and its temperature is stabilized to about 63.5 °C. A weak magnetic field (~150 mG) in the z direction of the atomic cell (parallel to line L_2) is applied by means of Helmholtz coils to provide a quantization axis. The $1/e$ intensity diameters of the probe, trigger, and coupling beams are about 1, 1, and 3 mm at the center of the cell, respectively. The probe and trigger beams are regained to their original linear polarizations after respectively passing through another $\lambda/4$ wave plate. The intensities of the probe, trigger, probe reference, and trigger reference beams are detected by detectors $D3$, $D2$, $D1$, and $D4$, respectively. The transmitted probe (s-polarized) and probe reference (p-polarized) beams from BS2 overlap each other at the exit of BD2 to be combined into beam P again. Similarly, the trigger (p-polarized) and trigger reference (s-polarized) beams are combined into another beam (T) at the exit of BD2. Then, the P (T) beam passes through a MgO:LiNbO$_3$ crystal Li1 (Li2) and a $\lambda/2$ wave plate. Similar to Ref. [14], the detectors $D7$ and $D8$ as well as $D5$ and $D6$ form two homodyne detectors, $H1$ and $H2$, respectively. The differential signals $\Delta I_{H1} \propto 2|E_{RP}||E_P|e^{-\alpha_P l/2} k n_P l$ and $\Delta I_{H2} \propto 2|E_{RT}||E_T|e^{-\alpha_T l/2} k n_T l$ from the $H1$ and $H2$ will give the probe and trigger dispersions $k n_P l$ and $k n_T l$, where E_{RP} ($\gg E_P$) and E_{RT} ($\gg E_T$) are the probe and trigger reference fields, respectively.

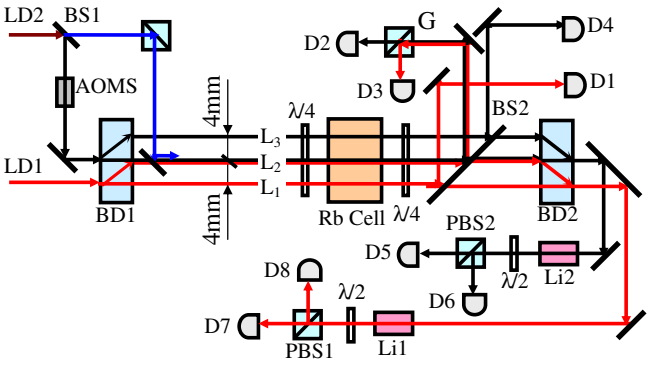

FIG. 1 (color online). Experimental setup.

We observed the EIT windows for probe and trigger fields when coupling detuning $\Delta_C = 0$. The powers of the coupling, probe, and trigger beams are set to $P_C =$ 14 mW ($\Omega_C \approx 70$ MHz), $P_P = 8$ μW ($\Omega_P \approx 3$ MHz), and $P_T = 10$ μW ($\Omega_T \approx 3$ MHz), respectively. When the coupling beam was on, we scanned the probe frequency across ω_{ae} to measure the probe absorption spectrum at $\Delta_T = 0$. An EIT window [Fig. 2(a)] for the probe beam, with a linewidth of ~2 MHz, appears at the resonance $\Delta_C = \Delta_P = 0$, which derives from the three-level Λ system $|b_3\rangle - |e_1\rangle - |a_2\rangle$ ($|b_4\rangle - |e_2\rangle - |a_3\rangle$). At $\Delta_P = 0$, scanning the trigger frequency around ω_{be} with the acousto-optical modulator system [12], the trigger EIT signal [Fig. 2(b)] at the resonance of $\Delta_C = \Delta_T = 0$ with

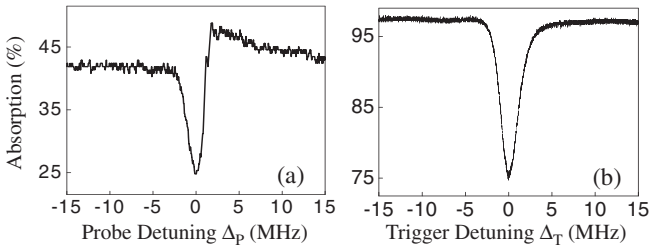

FIG. 2. The measured simultaneous EIT windows for (a) probe and (b) trigger beams created by a coupling beam with a power of 14 mW at detuning $\Delta_C = 0$.

a linewidth of ~2 MHz was observed, which derives from another three-level Λ system $|b_3\rangle - |e_1\rangle - |b_1\rangle$ ($|b_4\rangle - |e_2\rangle - |b_2\rangle$).

We also observed the cross-phase modulation between the probe and trigger fields under the conditions of different powers for the two beams. The measured results are shown in Fig. 3. During the measurements of Fig. 3, the coupling beam with a power of $P_C = 14$ mW was always on and the probe frequency was scanned across ω_{ae}. First, under the conditions $P_p = 8\ \mu$W and $P_T = 300\ \mu$W ($\Omega_T \approx 18$ MHz), i.e., $\Omega_P < \Omega_T (\ll \Omega_c)$, we measured the modulation of the probe field by the trigger field. The curves I of Fig. 3(a) and I' of Fig. 3(b), respectively, present the probe EIT absorption $\alpha_P(\omega_P)l$ and dispersion

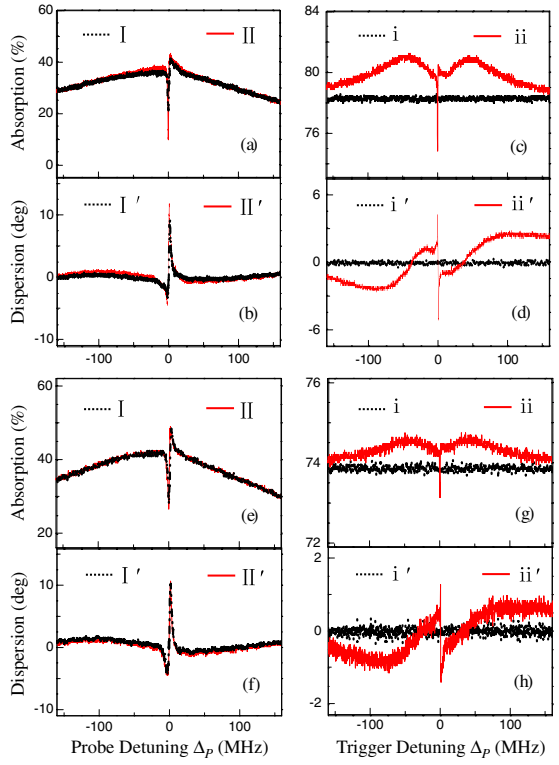

FIG. 3 (color online). The measured probe absorption [(a) and (e)] as well as dispersion [(b) and (f)], and trigger absorption [(c) and (g)] as well as dispersion [(d) and (h)] signals as the function of Δ_P for $\Delta_C = \Delta_T = 0$ and $Pc = 14$ mW.

$kn_P(\omega_P)l$ as the function of Δ_P when the trigger beam is blocked, which derive from the three-level Λ-type systems. When the trigger beam is applied, the four-level tripod systems are formed and the EIT window [curve II of Fig. 3(a)] and dispersion [curve II' of Fig. 3(b)] from the tripod systems become much larger than the corresponding results from the Λ-type systems, respectively. The top of the probe EIT window with the trigger beam is obvious beyond that without trigger beam, while in Ref. [12] this phenomenon did not occur. The reason is that the probe beam propagates through the Rb cell with a small angle relative to the trigger beam in Ref. [12], while, in the presented system, the two beams almost totally overlap. Thus, the interaction between two beams in the presented system is larger than that in Ref. [12]. From Fig. 3(b), we can see that the two EIT dispersion peaks of the probe beam occur at $\Delta_P \approx -0.7$ MHz and $\Delta_P \approx 0.6$ MHz, respectively. At the left (right) dispersion peak, a XPM phase shift Ψ_P^N of $\sim -2.5°$ (5°) was achieved, with a transmission of 70%. Next, we measured the modulation of the weaker trigger beam with a power of 10 μW by the stronger probe beam with a power of 300 μW. Traces i of Fig. 3(c) and i' of Fig. 3(d) present the trigger EIT absorption and dispersion $kn_Tl|_{I_P=0}$ signals when the probe beam is blocked, which correspond to the absorption and dispersion at resonance $\Delta_C = \Delta_T = 0$, respectively. Curves ii of Fig. 3(c) and ii' of Fig. 3(d) are the measured trigger EIT absorption and dispersion $kn_T(\omega_P)l|_{I_P\neq 0}$, respectively, when the probe beam is applied. The top of EIT in curve ii of Fig. 3(c) (four-level tripod systems) is far beyond the trace i of Fig. 3(c) (three-level systems) when both the probe and trigger fields are tuned to the dark states ($\Delta_C = \Delta_T = \Delta_P$). Simultaneously, a sharp EIT dispersion curve ii' of Fig. 3(d) appears at $\Delta_C = \Delta_T = \Delta_P = 0$, which is greatly different with that on the trace i' of Fig. 3(d). The trigger XPM phase shift can be calculated through $\Phi_T^N = k_T l(n_T|_{I_P\neq 0} - n_T|_{I_P=0})$ according to the data given from curves i' and ii' in Fig. 3(d). At $\Delta_P \approx \pm 0.5$ MHz, a maximum of the trigger XPM phase shift Φ_T^N of $\sim \pm 5°$ is achieved.

Successively, we observed the XPM between the weak probe and trigger fields, both of which have the same power $P_p \approx P_T \approx 14\ \mu$W ($\Omega_P \approx \Omega_T \approx 4$ MHz). Curves I of Fig. 3(e) and I' of Fig. 3(f) are the measured probe EIT absorption and dispersion without the trigger beam on, the curve i of Fig. 3(g) and i' of Fig. 3(h) are the measured trigger absorption and dispersion without the probe beam on. When the two beams were on, we simultaneously measured the EIT absorption curves II (probe) in Fig. 3(e) and ii (trigger) in Fig. 3(g), as well as the dispersion curves II' (probe) in Fig. 3(f) and ii' (trigger) in Fig. 3(h) in a scanning of Δ_p, respectively. The results show that the modulations of the probe EIT absorption and dispersion by the trigger beam are small, but the modulations of the trigger EIT absorption and dispersion by the probe beam are quite obvious. At $\Delta_P = \pm 0.5$ MHz, the

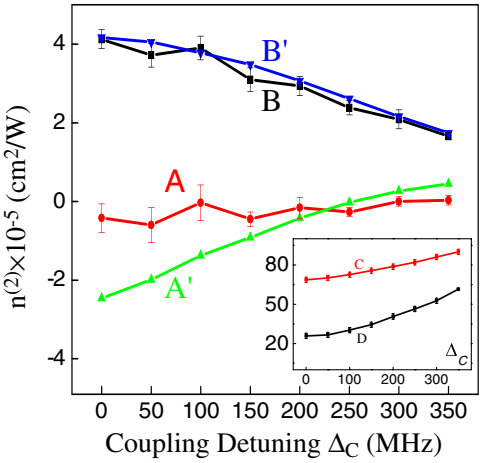

FIG. 4 (color online). Curves (A) and (B) are the measured probe and trigger XPM coefficients at $\Delta_P - \Delta_C \approx -0.5$ MHz as a function of Δ_C, respectively, for $P_P \approx P_T \approx 14$ μW. Curves (A') and (B') are corresponding theoretical results with experimental parameters $\gamma_0 = 3.5$ MHz, $\gamma_1 = 0.5$ MHz, $\gamma_2 = 1.5$ MHz, $\gamma_3 = 1.0$ MHz, $\Omega_C = 70$ MHz, $\Omega_P = \Omega_T = 4$ MHz, and $N = 3.72 \times 10^{11}/\text{cm}^3$. Curves ($C$) and ($D$) in the inset are the accompanying transmissions of probe and trigger beams at $\Delta_P - \Delta_C \approx -0.5$ MHz.

maximal trigger nonlinear phase shift $\sim \pm 1.4°$ is achieved with an absorption of $\sim$74%. However, such a large absorption is not desired in the practical application of QIP.

For exploring the optimal condition to obtain a large XPM and an accompanying small absorption, we measured the XPM phase shifts and the transmissions at the different Δ_C under the condition of the weak probe and trigger fields ($P_p \approx P_T \approx 14$ μW). Curves A and B of Fig. 4 plot the measured XPM coefficients $n_P^{(2)}$ and $n_T^{(2)}$ as the function of Δ_C. Curves C and D in the inset of Fig. 4 plot the simultaneously measured transmissions. Increasing Δ_C, the absolute values of XPM coefficients $n_P^{(2)}$ and $n_T^{(2)}$ go down, but the accompanying transmissions of the probe and trigger beams become larger, which allows the choice of an appropriate coupling frequency detuning to achieve substantial XPM phase shift with a smaller absorption. Figure 4 shows that $n_T^{(2)}$ is much larger than $n_P^{(2)}$. This asymmetry of $n_T^{(2)}$ and $n_P^{(2)}$ is not in agreement with the prediction in Ref. [2], in which the $n_T^{(2)} \leftrightarrow n_P^{(2)}$ exchange is symmetric. A possible reason is that the large differences between the probe Rabi frequencies ($\Omega_{P1} = \Omega_{P2} = 1.15$ MHz) and the trigger Rabi frequencies ($\Omega_{T1} = 2.83$ MHz, $\Omega_{T2} = 2$ MHz) could result in the difference of the populations of two ground state $|a_2\rangle$ and $|b_1\rangle$ ($|a_3\rangle$ and $|b_2\rangle$). In this case, the calculated populations with Eq. (3) of Ref. [12] are $\rho_{a2,a2} \approx 0.38$, $\rho_{a3,a3} \approx 0.3$, $\rho_{b1,b1} \approx 0.12$, and $\rho_{b2,b2} \approx 0.2$. At the same time, we theoretically calculated the fitting curves $n_P^{(2)}$ and $n_T^{(2)}$ at $\Delta_P - \Delta_C = -0.5$ MHz with Eq. (1), which are shown in curves A' and B'. The theoretical calculations are in reasonable agreement with the experimental results.

The enhanced XPM in the presented tripod system is based on simultaneous EIT for probe and trigger fields, and thus both the probe and trigger absorptions are small. For example, the trigger XPM coefficient can reach 2×10^{-5} cm^2/W with a transmission of $\sim$60% (see Fig. 4). Such a property is much better than that obtained with the N-type system, in which the probe EIT window will move into an absorption peak when a significant XPM phase shift is acquired [8]. If a probe beam with the intensity of $\sim$0.2 mW/cm^2 ($\Omega_P \approx 1$ MHz) is applied, which corresponds to the case that a probe pulse consisting of one photon is tightly focused to a spot size of a half wavelength at 795 nm, for a duration of 1 μs, the trigger XPM phase shift induced by the probe field will reach $\sim$0.0016 rad. Such a XPM phase shift may satisfy the requirement [5] of $\sqrt{n}\theta^2 \approx 5$ (the mean photon number n per pulse is on the order of 4×10^{12}); thus, the presented system may have practical applications in QIP based on a photon number quantum nondemolition detector [5,6]. Although the conditional phase shift which is defined as $\Phi_p^N + \Phi_T^N$ [1] in QPG still cannot reach $\sim\pi$ in our experimental conditions, if the laser linewidths of probe and trigger beams are suppressed down to 5 kHz, a conditional phase shift ($\Phi_p^N + \Phi_T^N$) based on the XPM between the two pulses with one photon will reach 1.2 rad for $\Omega_C = 30$ MHz, which may allow us to perform the QPG operation.

In summary, we have experimentally demonstrated the enhanced cross-Kerr nonlinearity based on double EIT. The double EIT windows are important for matching the group velocities of the probe and trigger beams, which produces an enhanced XPM between the two optical pulses [2].

We thank M. Xiao for helpful discussions and acknowledge the funding support by NSFC (60325414, 60578059, 60736040, 10640420195, and RGC60518001), and the 973 Program (2006CB921103).

*wanghai@sxu.edu.cn.

[1] Q. A. Turchette *et al.*, Phys. Rev. Lett. **75**, 4710 (1995).
[2] S. Rebic *et al.*, Phys. Rev. A **70**, 032317 (2004).
[3] A. Joshi *et al.*, Phys. Rev. A **72**, 062319 (2005).
[4] M. D. Lukin *et al.*, Phys. Rev. Lett. **84**, 1419 (2000).
[5] K. Nemoto *et al.*, Phys. Rev. Lett. **93**, 250502 (2004).
[6] S. D. Barrett *et al.*, Phys. Rev. A **71**, 060302(R) (2005).
[7] H. Schmidt *et al.*, Opt. Lett. **21**, 1936 (1996).
[8] H. Kang *et al.*, Phys. Rev. Lett. **91**, 093601 (2003).
[9] S. E. Harris *et al.*, Phys. Rev. Lett. **82**, 4611 (1999).
[10] David Petrosyan *et al.*, Phys. Rev. A **65**, 033833 (2002).
[11] Zeng-Bin Wang *et al.*, Phys. Rev. Lett. **97**, 063901 (2006).
[12] Shujing Li *et al.*, J. Phys. B **40**, 3211 (2007).
[13] Min Xiao *et al.*, Phys. Rev. Lett. **74**, 666 (1995).
[14] Yanxu Han *et al.*, Phys. Rev. A **77**, 023824 (2008).